The Stability and Dynamic Behavior of a Continuous Crystallizer with a Fines Trap

SHANG-JEN LEI, REUEL SHINNAR, and STANLEY KATZ

Department of Chemical Engineering
The City College, The City University of New York, New York, New York 10031

Working equations are developed for the operation of a continuous crystallizer with a fines trap. A linearized stability analysis reveals that proper operation of the fines trap can stabilize the crystallizer at large crystal product sizes that would otherwise lead to instability. Dynamic studies for the full nonlinear equations are carried out numerically, and stable limit cycles are exhibited around unstable equilibrium points.

Continuous removal of fines, or small crystals, from the crystal magma to increase the average particle size has become a standard practice in industrial crystallization (*2, 4, 5, 12, 13*). The fraction of fines removed is often quite high and may reach up to 30% of the production rate on a mass basis.

A schematic diagram of a typical fines trap is given in Figure 1 (*1, 12, 13*). Part of a mixed crystallizer is shielded by a baffle. The circulation of the magma through the baffled zone is slow and larger particles fall to the bottom. Only fine particles reach the top, from which a stream is drawn off to a heater, in which the smaller crystals are dissolved, or to a mechanical fines-removing device and the clear solution is fed back to the crystalline.

The design of the baffle and the crystallizer itself allows one to fix the maximum particle size r_0 that will be elutriated into the fines trap region. This design will determine the size distribution and magma density at the inlet to the fines trap. The amount of fines dispersion circulated through the fines trap w_0 is separately adjustable by the operator. The operator, in most cases, has very little direct control of r_0. In some designs, a change in w_0 also affects the maximum size which is elutriated into the fines zone, but here we will deal with the first case.

Fines traps are important tools in the control of the crystallizer. Not only do they allow adjustment of particle size at more or less constant production rate, but proper adjustment of the fines trap also allows one to stabilize the operation of the crystallizer (*1, 2*) and to prevent continued cycling.

Continued cycling of this kind is a serious problem in the scale up and operation of commercial continuous crystallizers (*1, 3, 8*). Quantitative treatment for both mixed and classified crystallizers (*15, 16*), in which the particle size fluctuates in a periodic way has been presented in two previous papers. A few cases of such cyclic operation are reported in the literature (*1, 3*), and in their industrial experience the authors have met with many examples such as the cycling crystallizer given in Figure 2.

The following analysis of both the steady state and the dynamic behavior of mixed crystallizers with fines traps should provide a theoretical background for a better understanding of their operation and design.

Correspondence concerning this paper should be addressed to Reuel Shinnar.

KINETICS OF NUCLEATION AND GROWTH

In any analysis of crystallizer behavior, the definition of the underlying kinetic regime is very important. Here we make the following assumptions:

1. The crystallizer itself is ideally mixed and the product removed is a representative fraction of the dispersion inside the crystallizer.

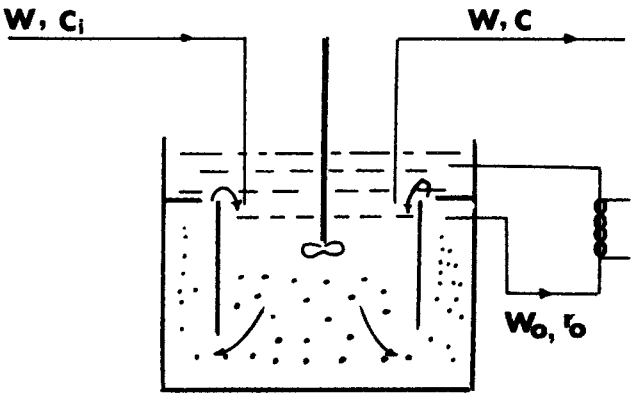

Fig. 1. A schematic diagram of a continuous crystallizer with a fines trap.

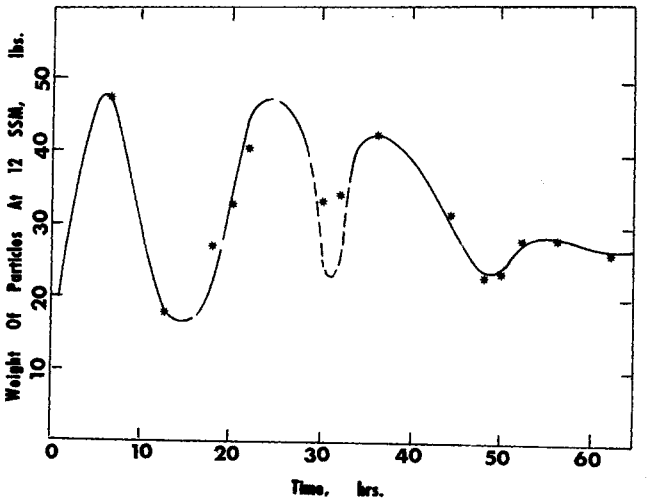

Fig. 2. Cycling in a continuous crystallizer.

2. The crystal growth rate is proportional to the supersaturation and is independent of particle size.

$$G = k_g\,(C - C_s) \tag{1}$$

3. The nucleation rate B is a function of supersaturation alone. For most cases the form suggested by Mier will be adopted:

$$B = k_b\,(C - C_m)^n \tag{2}$$

where C_m is some critical concentration level higher than the saturation concentration C_s, and n is an exponent $n \geq 1$.

If one limits oneself to a narrow range of growth rates then it is often possible to express this dependence as a simple power law (8). We might note at this point that all our results depend very strongly on Assumption 1 but that much of the mathematical analysis is independent of the particular rate expressions embodied in Assumptions 2 and 3.

These three are of course strong simplifying assumptions. References *1*, *6* to *8* show that even simple mixed crystallizers give size distributions which strongly differ from those predicted by Assumptions 1 and 2. (Assumption 3 has no effect on the steady state size distribution.) On the other hand, the problem is already very difficult in its simple form, and it was shown in reference *15* that if the growth rate is slightly nonlinear or size dependent it does not affect the basic results of the stability analysis.

The most critical assumption is the form of the dependence of nucleation rate on supersaturation or on growth rate. In a real crystallizer, nucleation occurs mostly by secondary nucleation and often by attrition. While these depend on the moments of the size distribution, the dependence is weak, and for stability purposes there is some justification in expressing the nucleation rate as a function of supersaturation (or growth rate) only.

Basically, we distinguish two cases of interest for crystallizers with fines traps. In the first case the nucleation sensitivity parameter (b/g), which is equivalent to the exponent in the local approximation of reference 8, is low, and therefore the size is insensitive to residence time. Control of particle size is possible only by a fines trap. The second case deals with crystallizers with high values of b/g under practical conditions. Equation (2) allows one to approximate both cases, and the general results can be applied to any case for which the kinetics is known. To illustrate this, $\ln B$ is plotted versus $\ln G$ in Figure 3 for Equation (2) as well as for a Volmer relation.

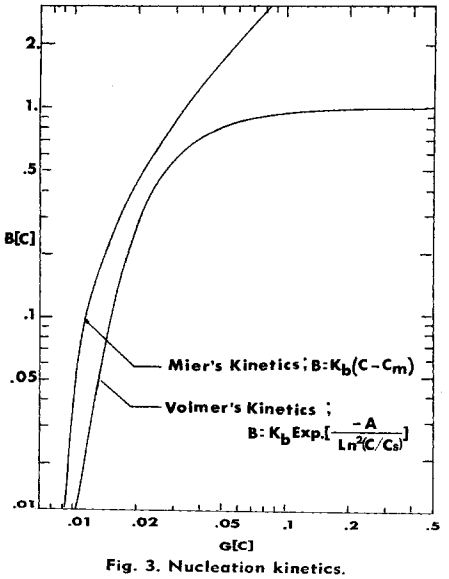

Fig. 3. Nucleation kinetics.

STEADY STATE RELATIONSHIPS

In this section, we set down the basic differential equations for a continuous crystallizer with fines trap and find their steady state solution. The results are illustrated by numerical examples based on the kinetics of Equations (1) and (2).

The crystals in the system are assumed to be geometrically similar solids; r is used as a characteristic linear dimension for the solid. The growth kinetics of Equation (1) are taken to apply to this linear dimension r, so that while a particle is in the system, $dr/dt = G$. A crystal of size r is taken to have volume kr^3, the parameter k serving as a particle shape factor. The dispersion in the crystallizer is characterized by a number density $f(r, t)$; that is, $f(r, t)dr$ is, at time t, the number of crystals per unit working volume of the crystallizer with sizes in the range $r, r + dr$. The fraction of the working volume occupied by solid is then $k\int_0^\infty r^3 \cdot f \cdot dr$, and the liquid fraction is accordingly

$$\epsilon(t) = 1 - k\int_0^\infty r^3 \cdot f(r, t)\,dr \tag{3}$$

We take the nucleation kinetics of Equation (2) to hold in this liquid volume only, so that, per unit working volume of the crystallizer, ϵB is the number of crystals formed per unit time. These nuclei are all taken to be of vanishingly small size. The kinetic functions B and G are dependent upon the solute concentration $c(t)$.

Now, from the schematic in Figure 1, we see that we may set down immediately an overall material balance on the system without taking explicit account of the fines trap operation:

$$\frac{d}{dt}\{\epsilon \cdot C + (1 - \epsilon) \cdot \rho\} = \frac{1}{\theta} C_i - \frac{1}{\theta}\{\epsilon \cdot C + (1 - \epsilon)\rho\} \tag{4}$$

Here, $\theta = v/w$ is the mean residence time of material in the unit. The feed to the crystallizer is taken to be clear liquid.

Describing the operation of the fines trap calls for the introduction of another characteristic time $\theta_0 = v/w_0$ to stand alongside the mean residence time θ. The quantity $1/\theta_0$ may be interpreted as a (probability) rate at which particles are circulated through the fines trap: that is, dt/θ_0 represents the fraction of particles circulated through the fines trap in a (short) time dt. A balance on particles of size r may accordingly be written in the form

$$\frac{\partial f}{\partial t} + G(c) \cdot \frac{\partial f}{\partial r} = \epsilon \cdot B(c) \cdot \delta(r) - \frac{1}{\theta} \cdot f - \frac{1}{\theta_0}\eta(r) \cdot f \tag{5}$$

The three terms on the right hand side of (5) represent respectively the formation of new crystals, the removal of crystal product, and the destruction of crystals in the fines trap. The function $\eta(r)$ represents a selection curve for fines destruction. We take it in the form

$$\eta(r) = h(r/r_0) = \begin{cases} 1\,; & \text{for } r < r_0 \\ 0\,; & \text{for } r > r_0 \end{cases} \tag{6}$$

The δ function in the nucleation term of Equation (5) represents the understanding that all new crystals are formed at size $r = 0$. Mathematically speaking, this term has the force of a boundary condition (at $r = 0$) for the partial differential Equation (5). We recognize accordingly that (5) can, so to speak, be expanded out into the more explicit form

$$G(c)f = \epsilon(t)B(c) \qquad r = 0$$

$$\frac{\partial f}{\partial t} + G(c)\frac{\partial f}{\partial r} = -\frac{1}{\theta}f - \frac{1}{\theta_0}\eta(r)f \quad r > 0 \qquad \text{(5 alt.)}$$

Equations (3) to (5) form a self-contained system for the determination of the solute concentration $c(t)$ and the particle number density $f(r, t)$. Besides the underlying assumptions about the nature of the kinetic regime discussed in the preceding section, their validity depends on two further assumptions. First, we take the system to be isothermal; the temperature does not appear explicitly, and there is no need to set down energy balances. Second, we neglect volume changes on crystallization, so that the system in fact operates at fixed volume v, with a common flow rate w in and out of the crystallizer and a common flow rate w_0 in and out of the fines trap. (The fines are redissolved in the destruction unit, not mechanically removed from the system.) The flow rates may of course change with time, and this change will be reflected in θ and θ_0.

We turn now to a consideration of the steady state solutions of the basic Equations (3) to (5). This offers no special difficulties, the ordinary differential Equation (4) reducing to an algebraic equation and the partial differential Equation (5) reducing to an ordinary differential equation. The solution to this ordinary differential equation in f is

$$f(r) = \epsilon\frac{B}{G}\cdot\exp\left\{-\frac{r}{\theta G} - \frac{1}{\theta_0 G}\int_0^r \eta(s)\,ds\right\} \qquad r \geq 0 \qquad (7)$$

Here, B and G are to be evaluated for the steady state concentration C, but we do not show this functional dependence explicitly. Bringing Equation (7) to (3) gives an explicit formula for ϵ

$$\epsilon = \frac{1}{1 + k\dfrac{B}{G}\displaystyle\int_0^\infty r^3 \exp\left\{-\frac{r}{\theta G} - \frac{1}{\theta_0 G}\int_0^r \eta(s)ds\right\}dr} \qquad (8)$$

and bringing this expression for ϵ to the steady state form of (4) gives

$$\frac{C_i - C}{\rho - C_i} = \frac{kB}{G}\int_0^\infty r^3 \exp\left\{-\frac{r}{\theta G} - \frac{1}{\theta_0 G}\int_0^r \eta(s)ds\right\}dr \qquad (9)$$

This is not an explicit formula for C, since B and G depend on C. One may see nevertheless that it is satisfied by only a single C since the left-hand side is a decreasing function of C and the right-hand side an increasing function (at least for any customary kinetics). Finally, from (7) we may evaluate the weight average crystal size

$$\bar{r} = \frac{\displaystyle\int_0^\infty r^4 \cdot f(r)dr}{\displaystyle\int_0^\infty r^3 \cdot f(r)dr}$$

in the crystallizer (and the product) as

$$\bar{r} = \frac{\displaystyle\int_0^\infty r^4 \exp\left\{-\frac{r}{\theta G} - \frac{1}{\theta_0 G}\int_0^r \eta(s)ds\right\}dr}{\displaystyle\int_0^\infty r^3 \exp\left\{-\frac{r}{\theta G} - \frac{1}{\theta_0 G}\int_0^r \eta(s)ds\right\}dr} \qquad (10)$$

Equations (9) and (10) summarize important aspects of the steady state behavior of the crystallizer. Given a knowledge of the physical system (ρ, k), of the kinetics (B and G as functions of C), of the feed (C_i), and of the fines trap operations (θ_0, η), these equations contain implicitly the dependence of G and B on C and hence on each other. To make these dependencies as explicit as may be, we first rewrite (9) and (10), making suitable changes of variables in the integrals and taking account of the form of η in (6):

$$\left.\begin{aligned}\bar{r} &= G\theta\cdot\frac{\nu_4}{\nu_3}\\ \frac{C_i - C}{\rho - C_i} &= kBG^3\theta^4\nu_3\end{aligned}\right\} \qquad (11)$$

with

$$\nu_n = \int_0^\infty x^n \exp\left\{-x - \frac{r_0}{\theta_0 G}\int_0^{\overline{\theta G x}/r_0} h(y)dy\right\}dx \qquad (12)$$

These relationships can perhaps be seen more clearly in dimensionless form. We normalize the rate functions B and G on their values B_i and G_i for the feed concentration C_i; we normalize the particle sizes $\bar{r}$, r_0 and the flow times θ, θ_0 on suitable constructs of these same inlet kinetic values B_i, G_i. That is, we set

$$\left.\begin{aligned}\theta &= \frac{\boldsymbol{\theta}}{(kB_iG_i^3)^{1/4}}, \quad \theta_0 = \frac{\boldsymbol{\theta}_0}{(kB_iG_i^5)^{1/4}}\\ \bar{r} &= \left(\frac{G_i}{kB_i}\right)^{1/4}\bar{\mathbf{r}}, \quad r_0 = \left(\frac{G_i}{kB_i}\right)^{1/4}\mathbf{r}_0\\ G &= G_i\mathbf{G}, \quad B = B_i\mathbf{B}\end{aligned}\right\} \qquad (13)$$

These dimensionless variables will be used throughout the rest of this section. We recognize that, according to the linear growth kinetics of Equation (1), the dimensionless G is simply

$$\mathbf{G} = \frac{C - C_s}{C_i - C_s}$$

and so may serve as a dimensionless measure of the supersaturation. The concentration C may be expressed in terms of this G, and we may accordingly regard the nucleation rate B as also expressed in terms of G. Bringing all this to (11), we find

$$\left.\begin{aligned}\frac{1 - \mathbf{G}}{L - 1} &= \mathbf{B}\mathbf{G}^3\boldsymbol{\theta}^4\nu_3\\ \bar{\mathbf{r}} &= \mathbf{G}\boldsymbol{\theta}\frac{\nu_4}{\nu_3}\end{aligned}\right\} \qquad (14)$$

where

$$L = \frac{\rho - C_s}{C_i - C_s}$$

The quantities ν_3 and ν_4 may still be taken from Equation (12), since expressions of the form $r/\theta G$ remain unaltered by the scale changes (13).

This is about as far as the development can be carried in general. To develop from (14) some general quantitative feelings about the effect of the fines trap parameters θ_0, r_0 on the crystallizer performance, we turn first to the important special case where the critical size r_0 is, in a suitable sense, small. If r_0 is very small as compared to the average particle size $\bar{r}$, the total mass contained in the distribution for all particles less than r_0 is negligible. Furthermore, the time needed for a nucleus to grow to size r_0 is very small as compared to θ. We can therefore, with some justification, assume that for very small values of $r_0/\bar{r}$ we may completely neglect the contribution of all particles less than r_0 to the mass balance and also assume that the destruction of nuclei in the fines trap is instantaneous. In mathematical terms, we implement these ideas by approximating η by $\eta(r) = r_0\delta(r)$ that is, approximating h, on consulting (6), by

$$h(y) = \delta(y)$$

To this approximation

$$\nu_n = n!\ \exp\left(-\frac{r_0}{\theta_0 G}\right) \tag{15}$$

and the Equations (14) can be solved in turn for θ and $\bar{r}$ in terms of G to give

$$\left.\begin{aligned} \theta &= \left\{\frac{1}{6(L-1)} \cdot \frac{1-G}{BG^3} \cdot \exp\left(\frac{r_0}{\theta_0 G}\right)\right\}^{1/4} \\ \bar{r} &= \left\{\frac{256}{6(L-1)} \cdot \frac{G(1-G)}{B} \cdot \exp\left(\frac{r_0}{\theta_0 G}\right)\right\}^{1/4} \end{aligned}\right\} \tag{16}$$

It will be convenient to have a form of words for this small r_0 approximation, and we shall say that (16) describes the behavior of a point fines trap, while the general Equations (14) and (12) describe the behavior of a finite fines trap. We see from (16) that the point fines trap approximation amounts simply to replacing the actual nucleation rate B by an effective nucleation rate $B \exp(-r_0/\theta_0 G)$, which depends explicitly on the growth rate G. Thus $1 - \exp(-r_0/\theta_0 G)$ represents the fraction of nuclei destroyed in the fines trap. This interpretation is quite consistent with the intuitive ideas about the smallness of r_0 noted above. While r_0/G, the time a nucleus needs to grow to size r_0, is small with respect to the mean residence time θ, it is finite with respect to the much smaller mean recirculation time θ_0. Indeed, for small r_0, the ratio r_0/θ_0 completely characterizes the operation of the fines trap.

The dimensionless Equation (16) may be regarded as the parametric representation of the $\bar{r} - \theta$ curves for a crystallizer with a point fines trap. To this approximation, as noted above, the two fines trap parameters r_0, θ_0 merge into a single parameter r_0/θ_0, and each choice of r_0/θ_0 leads to an $\bar{r} - \theta$ curve. The dimensionless growth rate G serves as the parameter in the parametric representation of these curves, and to make all complete we need to express B in terms of G. This can readily be done, and for the nucleation kinetics of (2) we find for the dimensionless B

$$B = \left(\frac{G - M}{1 - M}\right)^n; \quad n \geq 1 \tag{17}$$

where

$$M = \frac{C_m - C_s}{C_i - C_s}$$

Figure 4 shows a family of these curves with $L = 5$, $M = 1/400$, $n = 1$. We see from these curves how, for a given θ, $\bar{r}$ increases with the fines trap operating parameters r_0/θ_0. Since $r = 4G\theta$, this increase of $\bar{r}$ with r_0/θ_0 reflects a corresponding increase in the supersaturation. We see further from these curves how a given product size $\bar{r}$ can be attained in many different ways, by playing off θ against r_0/θ_0. The stability curves superimposed on Figure 4, and on Figures 5 to 7 following, will be developed and discussed in the next section of this paper.

The dimensionless Equation (16) for a point fines trap may also be examined from a somewhat different point of view. That is, we may regard

$$\lambda = \frac{r_0}{\theta_0 G} \tag{18}$$

as a single parameter describing the fines trap operation, in place of r_0/θ_0. This serves as a design rather than as an operating parameter for the fines trap, since in operation its value depends on the supersaturation actually attained in the crystallizer. A choice of λ thus represents a design decision to destroy a fraction $1 - e^{-\lambda}$ of the nuclei formed. Bringing Equation (18) to (16) accordingly gives the parametric representation of a family of $\bar{r} - \theta$ curves

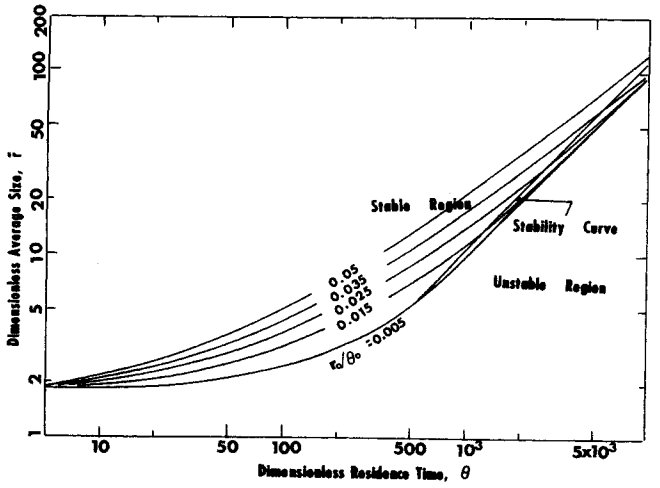

Fig. 4. Illustrative operating curves for a crystallizer with a point fines trap.

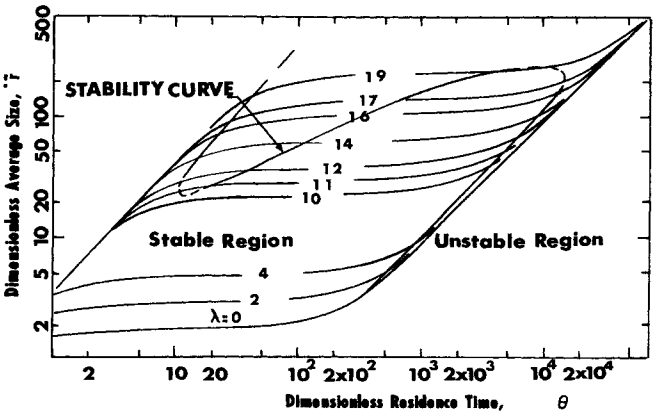

Fig. 5. Illustrative design curves for a crystallizer with a point fines trap.

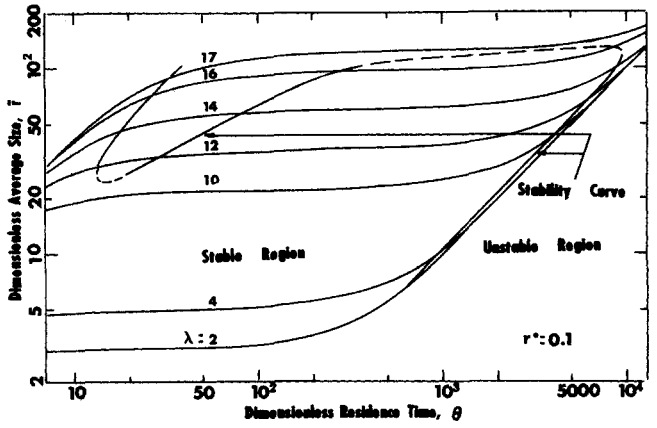

Fig. 6. Illustrative design curves for a crystallizer with a finite fines trap.

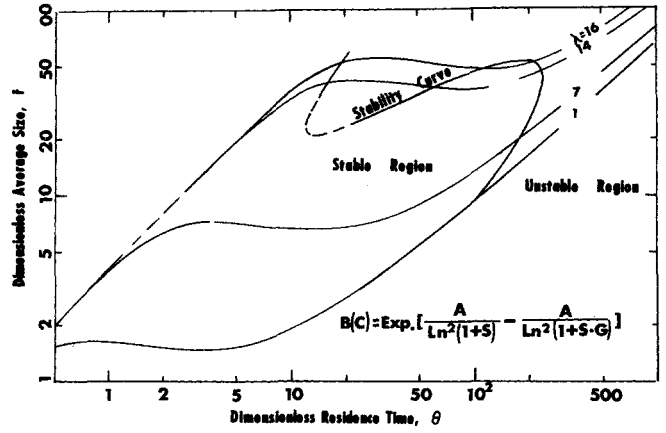

Fig. 7. Characteristic curves for a crystallizer with a point fines trap for Volmer's kinetics.

$$\theta = \left\{ \frac{1}{6(L-1)} \cdot \frac{1-G}{BG^3} \cdot e^{\lambda} \right\}^{1/4}$$
$$\bar{r} = \left\{ \frac{256}{6(L-1)} \cdot \frac{G(1-G)}{B} \cdot e^{\lambda} \right\}^{1/4} \tag{19}$$

that we may interpret as design curves for a crystallizer with point fines trap. A family of these curves is shown in Figure 5, with the nucleation kinetics of (17) and the same values of L, M, n as in Figure 4. These curves show the same general behavior as those of Figure 4. (Equivalent results for power law kinetics are given in reference *10*.)

We turn next to a consideration of how the general character of the curves of Figures 4 and 5 is affected by relaxing the small r_0 assumption that leads to a point fines trap. We shall not analyze this in great detail but shall simply illustrate the effects by showing some typical cases. We bring (18) to (12) and write

$$\nu_n = \int_0^{\infty} x^n \cdot \exp\left\{ -x - \lambda \int_0^{x/r^*} h(y)\,dy \right\} dx \tag{20}$$

where we have set

$$\frac{r_0}{\theta G} = r^* \tag{21}$$

We note that $r^* = 0$ for the point fines trap. With r^* as a free parameter in place of r_0, the quantities ν_n no longer depend on θ, and we may solve the Equations (12) for θ and $\bar{r}$ directly in terms of G:

$$\theta = \left\{ \frac{1}{L-1} \cdot \frac{1-G}{BG^3} \cdot \frac{1}{\nu_3} \right\}^{1/4}$$
$$\bar{r} = \left\{ \frac{1}{L-1} \cdot \frac{G(1-G)}{B} \cdot \frac{\nu_4^4}{\nu_3^5} \right\}^{1/4} \tag{22}$$

Equations (22) and (20) thus give the finite fines trap behavior corresponding to the point fines trap Equations (19). Figure 6 shows the results of some typical calculations. We see there how the behavior of the system varies with λ for a fixed r^*. The plots are made with the nucleation kinetics (17) and the same values of L, M, n as in Figures 4 and 5.

We may note finally that the general monotone character of the curves of Figures 4 and 5 does not depend on the particular numerical values chosen there for illustration. As long as we stay with the nucleation kinetics (17) that correspond to (2), $\bar{r}$ will increase steadily with θ on each curve, and the general configuration will be as shown. This will also be the case if the nucleation rate is a simple power of the supersaturation, that is, in our dimensionless variables, if $B = G^n$ with $n \geq 1$. But it need not be true for other common forms in which one describes the nucleation rate. With Volmer kinetics, for example, where we have for the nucleation rate in its customary physical units

$$B = k_b \exp\left[\frac{-A}{\ln^2\left(\frac{C}{C_s}\right)} \right] \tag{23}$$

we may for suitable choices of parameters find a downturn in the $\bar{r} - \theta$ curve followed by a later upswing.

In terms of our dimensionless variables, the nucleation kinetics (23) may be written

$$B = \exp\left\{ \frac{A}{\ln^2(1+S)} - \frac{A}{\ln^2(1+SG)} \right\} \tag{24}$$

where

$$S = \frac{C_i - C_s}{C_s}$$

For comparison with Figure 5, Figure 7 shows an $\bar{r} - \theta$ plot for a point fines trap with the nucleation kinetics (24) for various λ. All the curves are for $L = 5$, $S = 1$, $A = 5 \times 10^{-3}$. The existence of the local maxima and minima in these curves depends on the particular values of the parameters chosen, and the curves can be made monotone by taking, for example, a somewhat larger value of A.

This phenomenon of $\bar{r}$ falling as θ increases over a suitable range is not particularly a question of fines trap operation but rather of the form of the nucleation kinetics. It may be observed for a simple mixed crystallizer, and indeed taking $r_0/\theta_0 = 0$ in (16) or $\lambda = 0$ in (19) or, more generally, $h(y) = 0$ in (12) and (14) leads to a common set of equations

$$\theta = \left\{ \frac{1}{6(L-1)} \cdot \frac{1-G}{G^3B} \right\}^{1/4}$$
$$\bar{r} = \left\{ \frac{256}{6(L-1)} \cdot \frac{G(1-G)}{B} \right\}^{1/4} \tag{25}$$

describing the behavior of a mixed crystallizer without a fines trap. Curves based on Equation (25) show the same behavior. The existence of regions in which $\bar{r}$ decreases as θ increases has been predicted (*8*) for certain kinds of power law kinetics (with exponent < 1) and has in fact been observed in practice (*3*).

One can also use Figures 4 to 7 to understand the effect of a fines trap on crystallizers with power law kinetics. Equation (17) for $\mathbf{G} >> M$ reduces to $B = G^n$, and for this case b/g will be equal to n. For our example $n = 1$, and one would therefore expect (8) that for $\mathbf{G} >> M$ particle size becomes independent of θ, which in our example is true for $\boldsymbol{\theta} < 100$. For large θ, the supersaturation becomes small and approaches asymptotically the metastable limit. b/g increases without bound. For high values of θ, all the curves $r(\theta)$, have a linear asymptote $\bar{r} = 4\mathbf{G}\boldsymbol{\theta}$. Similar considerations hold for the Volmer model for very high supersaturations. $\mathbf{B}$ becomes independent of $\mathbf{G}$, and therefore $\bar{r}$ decreases with increasing $\boldsymbol{\theta}$. At high values of θ the supersaturation drops and one again notes that Equation (2) approximates the basic behavior of the Volmer relation very well. In the region of high supersaturation, introducing a point fines trap changes the dependence of the effective nucleation rate B_{eff} on G, as the probability of a nucleus surviving till r_0 depends on G. We note therefore that at constant fines trap setting (constant $\mathbf{r_0/\theta_0}$), $\bar{r}$ is now a function of $\boldsymbol{\theta}$. It is hard to express this new dependence as a power law, as in this case

$$\frac{\mathbf{b}}{\mathbf{g}_{\text{eff}}} = \frac{d\ln B_{\text{eff}}}{d\ln G} = (b/g)_{r_0=0} + \frac{r_0}{\theta_0 G}$$

LINEARIZED STABILITY ANALYSIS

In this section, we develop stability criteria for the operation of a continuous crystallizer with a fines trap. The results, expressed in terms of suitable dimensionless parameters characterizing the steady state operating point under study, are applied to the steady state operating and design curves developed in the preceding section. Mathematically speaking, the methods are entirely those of linear analysis.

Our starting point here is the basic set of differential Equations (3) to (5), with the variables all in their customary physical units. It is convenient to rewrite them in terms of a total solute-crystal resource function:

$$\varphi(t) = \epsilon(t) \cdot C(t) + (1 - \epsilon(t)) \cdot \rho \tag{26}$$

so that, consulting (3)

$$C = \frac{\varphi - \rho \cdot k \cdot \int_0^\infty r^3 \cdot f \cdot dr}{1 - k\int_0^\infty r^3 f \cdot dr} \tag{27}$$

and the Equations (4) and (5) give in turn

$$\frac{d\varphi}{dt} = \frac{1}{\theta}(C_i - \varphi) \tag{28}$$

$$\left.\begin{aligned} G(c) \cdot f &= \left(1 - k\int_0^\infty r^3 f\right) \cdot B(c); \quad r = 0 \\ \frac{\partial f}{\partial t} + G\frac{\partial f}{\partial r} &= -\frac{1}{\theta} \cdot f - \frac{1}{\theta_0} \cdot \eta(r) \cdot f; \quad r > 0 \end{aligned}\right\} \tag{29}$$

We now linearize Equations (27) to (29) about the steady state solution of the preceding section; that is, we carry

$$\varphi(t) \to \varphi + \delta\varphi(t)$$

$$C(t) \to C + \delta C(t)$$

$$f(r, t) \to f(r) + \delta f(r, t)$$

where C and $f(r)$ are given in Equations (7) to (9) and the corresponding φ by (26). The functions $\delta\varphi$, δC, and δf are regarded as small perturbations, and so their squares and products may be neglected. The details are tedious but straightforward, and we omit them here. The variable δC can be eliminated altogether by consulting the linearized form of (27), and we are left with

$$\frac{d(\delta\varphi)}{dt} + \frac{1}{\theta} \cdot \delta\varphi = 0 \tag{30}$$

from (28) and

$$\left.\begin{aligned} &G \cdot \delta f + \left\{1 + (\rho - C)\left(\frac{B'}{B} - \frac{G'}{G}\right) \cdot B \cdot k\int_0^\infty r^3\,\delta f\right\} = \left(\frac{B'}{B} - \frac{G'}{G}\right) B \cdot \delta\varphi; \quad r = 0 \\ &\frac{\partial(\delta f)}{\partial t} + G\frac{\partial(\delta f)}{\partial r} + \left(\frac{1}{\theta} + \frac{\eta}{\theta_0}\right) \cdot \delta f \\ &\quad + \left(\frac{1}{\theta} + \frac{\eta}{\theta_0}\right) e^{-\frac{r}{\theta G} - \frac{1}{\theta_0 G}\int_0^r \eta/(\rho - C)\,\cdot} \\ &\quad \frac{G'}{G}\frac{B}{G}k\int_0^\infty r^3\,\delta f = \left(\frac{1}{\theta} + \frac{\eta}{\theta_0}\right) \cdot \\ &\quad e^{-\frac{r}{\theta G} - \frac{1}{\theta_0 G}\int_0^r \eta}\frac{G'}{G}\frac{B}{G}\delta\varphi; \quad r > 0 \end{aligned}\right\} \tag{31}$$

from (29). Here B and G are the values of the nucleation and growth rates at the steady state under study, and B' and G' the values of their derivatives (with respect to the concentration C) at this steady state.

It is convenient at this point to introduce dimensionless variables into (30, 31). We set

$$\begin{aligned} t &= \theta \mathrm{t} \\ r &= \theta G \mathrm{r} \\ \delta f &= \epsilon \frac{B}{G}\,\delta \mathrm{f} \\ \delta\varphi &= 6k\epsilon\frac{B}{G} \cdot (G\theta)^4 \cdot (\rho - C) \cdot \underline{\delta\varphi} \end{aligned} \tag{32}$$

where the quantities C, ϵ, B, G are evaluated for the steady state under study. We may note a difference between this scaling and that made in Equation (13) for the analysis of steady state behavior; here quantities are scaled in terms of the steady state being studied; there, in terms of feed parameters. At any rate, the dimensionless variables of Equation (32) will be used throughout the remainder of this section. And in terms of them, we have

$$\frac{d(\delta\varphi)}{dt} + \underline{\delta\varphi} = 0 \tag{33}$$

from (30) and

$$\delta \mathrm{f} + (b - g)\int_0^\infty \frac{\mathrm{r}^3}{6} \cdot \delta \mathrm{f} = /(b - g - \alpha)\underline{\delta\varphi}; \quad \mathrm{r} = 0$$

$$\frac{\partial(\delta \mathrm{f})}{\partial \mathrm{t}} + \frac{\partial(\delta \mathrm{f})}{\partial \mathrm{r}} + (1 + R \cdot \eta) \cdot \delta \mathrm{f}$$

$$+ g\,(1 + R\eta)e^{-\mathrm{r} - R\int_0^{\mathrm{r}} \eta \int_0^\infty \frac{\mathrm{r}^3}{6}}\,\underline{\delta \mathrm{f}}$$

$$= g\,(1 + R \cdot \eta) e^{-r - R\int_0^r \eta} \quad \underline{\delta\varphi}; \quad r > 0 \tag{34}$$

In the dimensionless form given by Equations (33, 34), the linearized behavior of the crystallizer with a fines trap depends on a number of dimensionless parameters. We have for the system overall the nucleation and growth-rate sensitivity parameters

$$b = 6kBG^3\theta^4 \left\{ 1 + (\rho - C)\frac{B'}{B} \right\}$$
$$g = 6kBG^3\theta^4 (\rho - C)\frac{G'}{G} \tag{35}$$

as well as the auxiliary parameter

$$\alpha = 6kBG^3\theta^4$$

(which will not in fact appear in the stability conditions to be developed). For the fines trap itself, we have the recirculation ratio

$$R = \frac{\theta}{\theta_0} = \frac{W_0}{W} \tag{36}$$

and the knowledge of the critical fines destruction size contained in the selection curve $\eta(r)$. (This last will be brought out explicitly later.)

Our stability analysis for the system is based on Equations (33) and (34). We carry it out here by a formal spectral (eigenvalue) analysis, which we feel is free of some of the ambiguities of the customary Laplace transform methods. Since these spectral methods may be of some interest in related problems, we lay them out for Equations (33) and (34) in the Appendix and simply quote the results here. The upshot of the argument is that the characteristic equation for (33) and (34) is given by

$$1 + (b - g)\,H(s) + g \cdot K(s) = 0 \tag{37}$$

with

$$H(s) = \int_0^\infty \frac{r^3}{6} \cdot \exp\left\{ -(s+1)\,r - R\int_0^r \eta(x)\,dx \right\} dr$$
$$K(s) = \int_0^\infty \frac{r^3}{6} \exp\left\{ -(s+1)r - R\int_0^r \eta(x)\,dx \right\} \cdot \left(\frac{e^{sr} - 1}{s} + R\int_0^r \eta(y)\, e^{sy}\, dy \right) \cdot dr \tag{38}$$

we accordingly set

$$\eta(r) = h(r/r^*)$$

where

$$h(x) = \begin{cases} 1; & x < 1 \\ 0; & x > 1 \end{cases} \tag{39}$$

We note from (36) and (21) that

$$Rr^* = \lambda \tag{40}$$

the parameter introduced in (18) to characterize the steady state operation of the fines trap. The functions H and K of (38) may now be written

$$H(s) = \int_0^\infty \frac{r^3}{6} \exp\left\{ -(s+1)\,r - \lambda\int_0^{r/r^*} h(x)\,dx \right\} dr$$
$$K(s) = \int_0^\infty \frac{r^3}{6} \exp\left\{ -(s+1)r - \lambda\int_0^{r/r^*} h(x)\,dx \right\} \cdot \left(\frac{e^{sr} - 1}{s} + \lambda\int_0^{r/r^*} h(y)\, e^{syr^*} dy \right) \cdot dr \tag{41}$$

While in (41) the fines trap is described in terms of the parameters λ and r^*, we see from (40) that any two of the three parameters R, r^*, λ could equally well be used.

The form of H and K in Equation (41) is not especially transparent, and to develop some quantitative feeling about the stability condition based on (37), we turn first, as in the steady state studies of the preceding section, to the important special case of the point fines trap. We let $r^* \downarrow 0$ in (41), keeping λ fixed; from (40), we see that R must $\uparrow \infty$. The functions H and K become simple rational functions of s, and the characteristic Equation (37) reduces to

$$s^4 + (4 + ge^{-\lambda})s^3 + (6 + 4ge^{-\lambda})s^2 + (4 + 6ge^{-\lambda})s + \{1 + 3ge^{-\lambda} + (b + \lambda g)e^{-\lambda}\} = 0 \tag{42}$$

The polynomial character of (42) makes matters especially simple, and a straightforward application of the Routh-Hurwitz criterion shows that the system will be stable provided only that

$$g > -4e^{\lambda}$$

$$b < \frac{(21 - \lambda)g^3 + (87 - 8\lambda)e^{\lambda}g^2 + (128 - 16\lambda)e^{2\lambda}g + 64e^{3\lambda}}{(g + 4e^{\lambda})^2} \tag{43}$$

The characteristic Equation (37) determines formally the eigenvalues S associated with the system (33) and (34), and the stability condition for the system is accordingly that all the roots of (37) have negative real parts.

We now introduce explicitly the dependence of η on the critical fines destruction size r_0. According to Equation (6), $\eta(r) = h(r/r_0)$ where r and r_0 are in their ordinary physical units. If r is taken in the dimensionless form given by (32), then r_0 must be so taken also. That is, r_0 must be replaced by $r_0/\theta G$. But this is simply the r^* of Equation (21), and in the dimensionless variables of (32) (which will of course always be satisfied) and further that By introducing a function σ to represent the stable limit

$$\sigma(g) = \frac{21g^3 + 87g^2 + 128g + 64}{(g + 4)^2} \tag{44}$$

we may rewrite the stability condition (43) in a form that shows more clearly the natural groupings of the crystallizer parameters

$$(b + \lambda g)e^{-\lambda} < \sigma(ge^{-\lambda}) \tag{45}$$

The stability condition (45) is shown graphically in Figure 8. We may note that on setting $\lambda = 0$ we recover

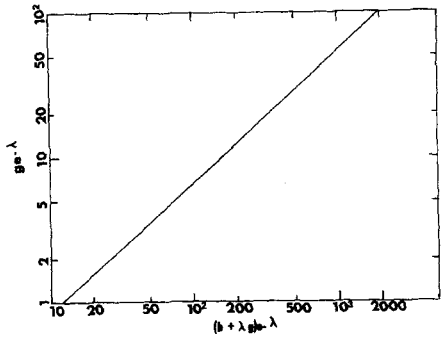

Fig. 8. General stability condition for a crystallizer with a point fines trap.

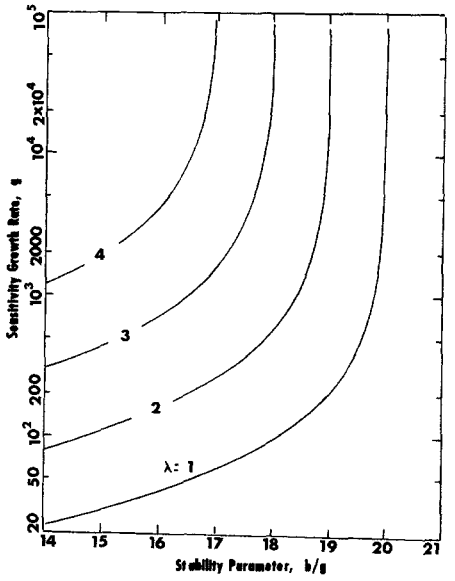

Fig. 9. Working stability curves for a crystallizer with a point fines trap.

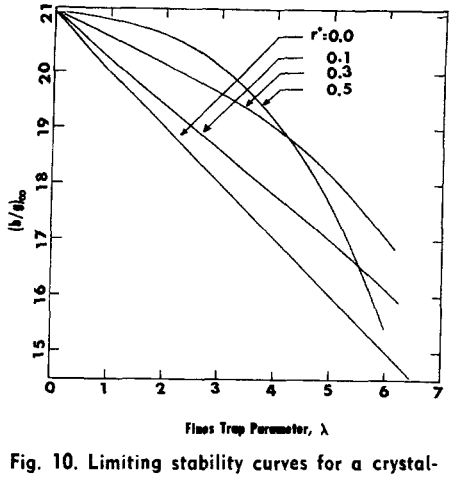

Fig. 10. Limiting stability curves for a crystallizer with a finite fines trap.

the stability condition for a mixed crystallizer without a fines trap, since in (41), setting $\lambda = 0$ is entirely equivalent to setting h, that is η, identically $= 0$. While Figure 8 embodies the general stability condition for a crystallizer with a point fines trap, it may be useful for certain working purposes to replot it in a somewhat more explicit form. We see from (43) that just on the verge of instability, b/g has a limiting value $= 21 - \lambda$ as $g \uparrow \infty$, and so the larger we take λ (the more fines we destroy), the smaller we must take b/g to ensure stable operation. The approach to this limiting value is not uniform; that is, the larger we take λ, the larger we must take g to approximate the limiting behavior of b/g. This whole state of affairs is shown graphically in Figure 9.

The stability curves overlying the steady state characteristic curves of Figures 4, 5, and 7 for a crystallizer with a point fines trap may be developed directly from the foregoing stability conditions. When the curves of Equation (16) are plotted to give Figure 4 or those of (19) are plotted to give Figure 5, it is necessary, for each value of the parameter $\mathbf{G}$, to merely compute the sensitivity parameters b and g of (35) and to consult the stability condition of (43) or (45). These sensitivity parameters can be directly expressed in terms of the dimensionless quantities of the preceding section. For the Mier nucleation kinetics of (17), we have

$$\left.\begin{aligned} b &= 6\left(\frac{\mathbf{G}-M}{1-M}\right)^n \mathbf{G}^3\,\boldsymbol{\theta}^4\left(1+n\frac{L-\mathbf{G}}{\mathbf{G}-M}\right) \\ g &= 6\left(\frac{\mathbf{G}-M}{1-M}\right)^n \mathbf{G}^3\,\boldsymbol{\theta}^4\frac{L-\mathbf{G}}{\mathbf{G}} \end{aligned}\right\}$$

where $\mathbf{G}$ and $\boldsymbol{\theta}$ are the dimensionless quantities of (13), and L is the dimensionless parameter introduced in (14). In the curves of Equation (16) that lead to Figure 4, λ must be computed as $\mathbf{r}_0/\boldsymbol{\theta}_0\mathbf{G}$ for each choice of G in order to enter the stability condition. In the curves of Equation (19) that lead to Figure 5, λ already appears explicitly. Similar considerations apply for the Volmer kinetics on which the curves of Figure 7 are based.

Reexamining the steady state curves of Figures 4 and 5 in the light of these superimposed stability conditions shows how a fines trap may permit the stabilizing of a crystallizer operation without the sacrifice of product quality. From the design curves of Figure 5, for example, we may see that when a desired product size $\bar{\mathbf{r}}$ leads to unstable operation in a crystallizer without a fines trap ($\lambda = 0$), a crystallizer with a fines trap may be designed to give stable operation with the same $\bar{\mathbf{r}}$. The required mean residence time $\boldsymbol{\theta}$ will be shorter in the crystallizer with a fines trap, and the design value of the crystallizer volume correspondingly smaller for a desired production rate. Corresponding conclusions about the operation of an existing fines trap may be drawn from Figure 4; here $\mathbf{r}_0/\boldsymbol{\theta}_0 = 0$ represents operation without the fines trap.

We turn now to a consideration of how the character of the stability curves of Figure 9 is modified on relaxing the condition $r^* = 0$ that leads to a point fines trap. Our starting point is the characteristic Equation (37) with the general H and K of (41) for a finite fines trap. With h given by (39), the functions H and K are no longer simply rational functions of s, but involve as well delay terms e^{-sr^*}. The details are not shown here, but the upshot is that the characteristic equation for a finite fines trap takes the form

$$P(s) + Q(s)e^{-sr^*} = 0 \qquad (46)$$

where P and Q are polynomials in s, with coefficients depending on b, g, r^* and λ (or R). There are of course various ways of extracting stability conditions from characteristic equations like (46). Our primary method was to find those relations among the parameters b, g, r^*, λ for which (46) has purely imaginary roots s and to interpret these relations as stabilizing limits. For fixed r^* and λ, this leads to curves in the b — g plane which may be compared with the point fines trap curves and with curves obtained by various approximative methods. All the curves

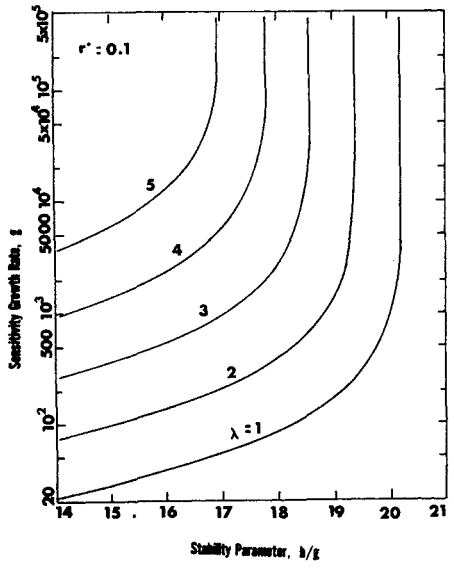

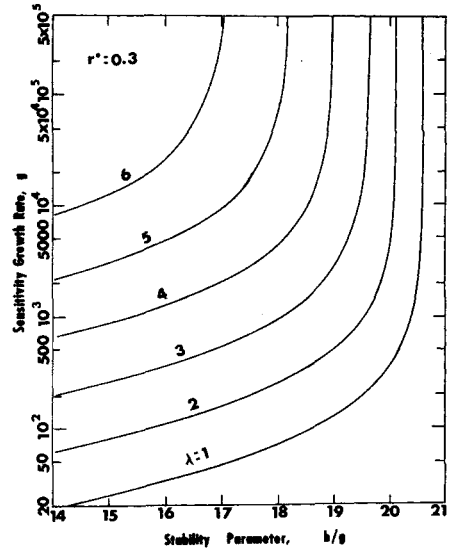

Fig. 11. Illustrations of the effect of fines destruction rate on the stability curves for a crystallizer with a finite fines trap.

so obtained showed limiting values of b/g for large g; we recall that for the point fines trap, $r^* = 0$, the limiting value is $(b/g)_\infty = 21 - \lambda$. Figure 10 summarizes our numerical results in this area by showing how this limiting value $(b/g)_\infty$ depends on the fines trap parameters λ and r^*.

Typical shapes of the full $b - g$ stability curves are shown in Figures 11 and 12. Figure 11 illustrates the orderly progress of these curves as the parameter λ and hence the recirculation ratio R are raised for fixed r^*. The limiting value $(b/g)_\infty$ goes steadily down as λ goes up. Figure 12 illustrates the more complicated advance and retreat of the curves with r^* for fixed λ. Here $(b/g)_\infty$ rises to a maximum as r^* goes up from 0 and then decreases; the behavior as r^* nears unity (not shown here) becomes very complicated. The stability curve superimposed on the steady state curves of Figure 6 was taken from Figure 12 in the manner described earlier for the point fines trap curves. Its shape opens up the interesting possibility that with λ chosen, perhaps, from the considerations mentioned earlier there is a value of r^* which gives the largest stable margin for the operation of the fines trap.

NONLINEAR DYNAMIC BEHAVIOR

In this section, we present the results of some numerical solutions of the full nonlinear dynamic Equations (3) to (5). All calculations are made about some steady state operating point. Their purpose is primarily to verify the linearized stability analysis of the preceding section, by following the propagation of finite perturbations from various steady state solutions. From these numerical investigations, we conclude that a linearly stable operating point is stable for the most part and that a linearly unstable operating point has associated with it a stable limit cycle.

The calculations have also another purpose: to follow the stabilizing effect of fines destruction (which was noted earlier) under comparable feed and product conditions for the system as a whole. To this end, cases for presentation are not chosen at random, but rather must have the same inlet conditions and the same mean product size. The precise form in which the equations are taken for solution and the details of the numerical procedures have been omitted here.

We present here a number of cases, all with the same dimensionless steady state mean crystal size of (13), $\bar{r} = 5$, and all with the parameter L of (14) equal to 5. These cases are all calculated for the kinetics of (17), with $M = 0.0025$, $n = 1$. Since the zeroth moment of $f(r, t)$ most sensitively shows the effects we are looking for, we present only plots of its perturbation $\delta\mu_0$ (taken in units of the steady state zero moment) against the time t (taken in units of the mean residence time). The curves presented here are for initial perturbations from steady state values in supersaturation and for certain corresponding perturbations in the size distribution made to give a smoother mathematical response.

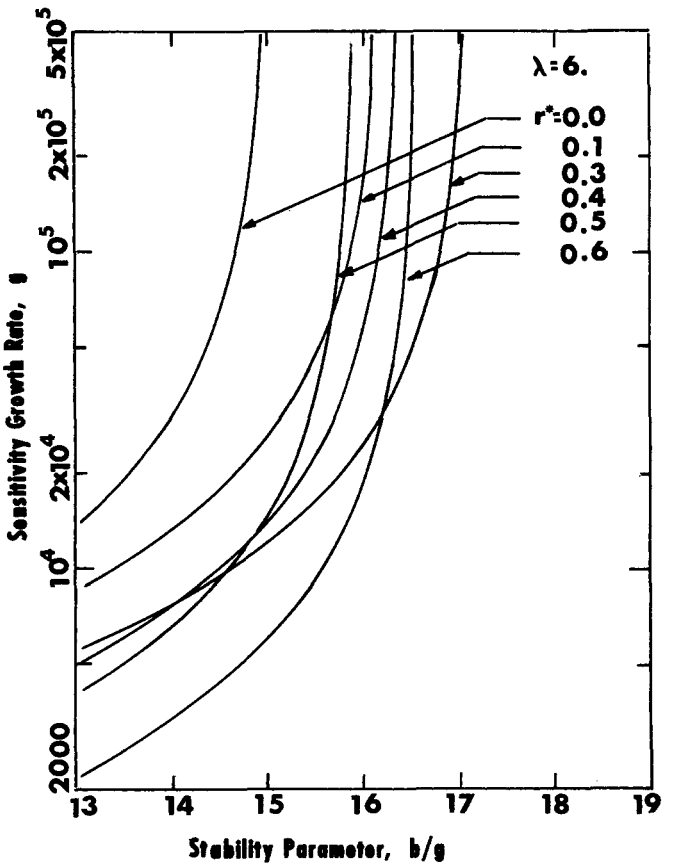

Fig. 12. Illustrations of the effect of fines destruction size on the stability curves for a crystallizer with a finite fines trap.

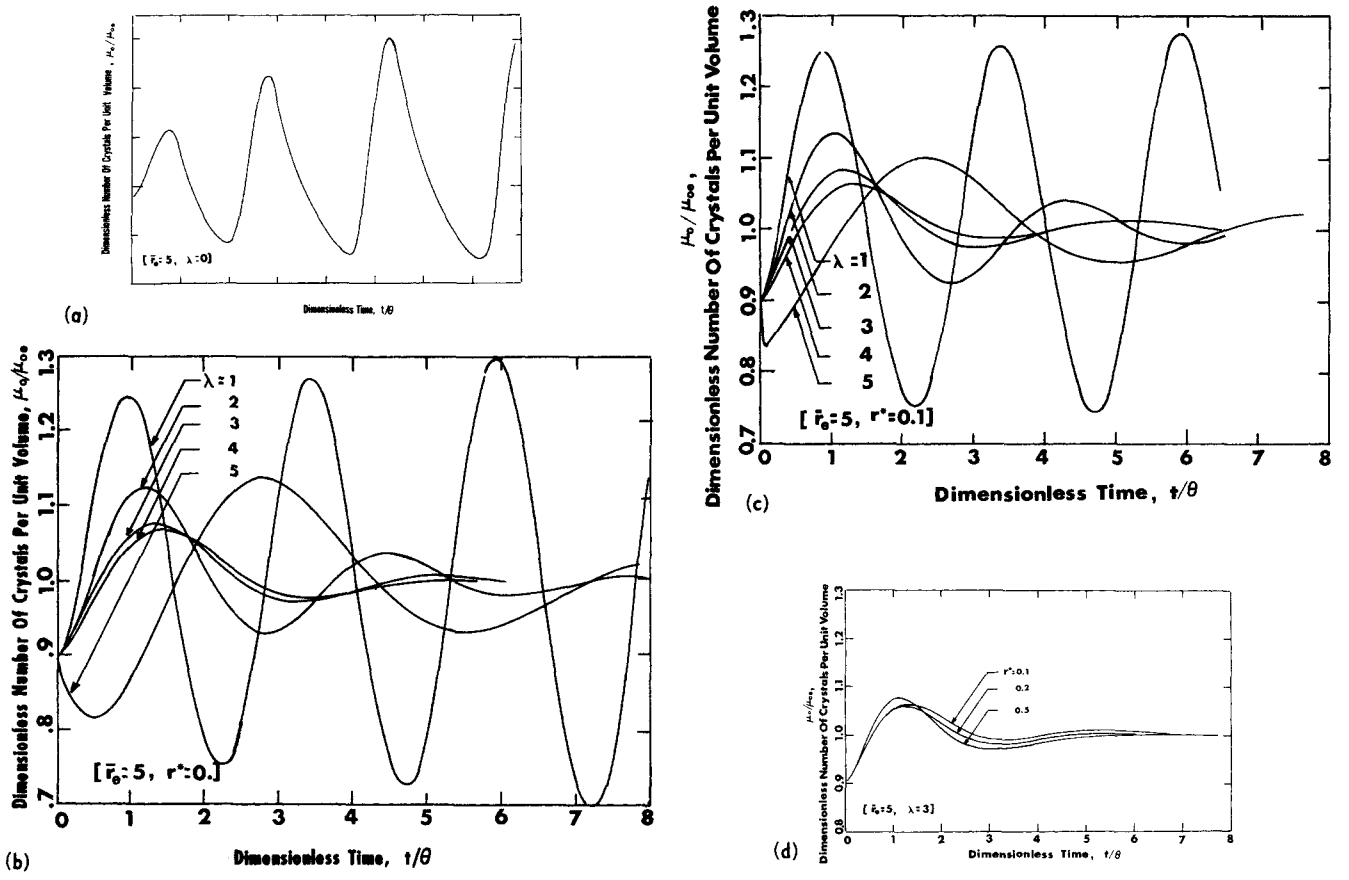

Fig. 13 Illustrative dynamics of a crystallizer with a finite fines trap.

Under these conditions, $\bar{r} = 5$ gives unstable operation for a crystallizer without a fines trap, and the curves of Figure 13*a* show how the instability leads to continued cycling in the absence of enough fines trap action, and how the cycling is damped by suitable fines trap action (Figures 13*b*, 13*c*).

It is particularly interesting to observe how the behavior of the nonlinear system is correctly predicted by the linear stability analysis and how the behavior of the nonlinear system calculated by the finite fines trap model can be represented by the calculation based on the point fines trap (when the critical size r^* is small). It is also important to note that the r^* which leads to the largest stable margin for fixed λ gives the best response in the nonlinear calculation (Figure 13*d*).

DISCUSSION

The previous sections offered some typical general examples of the effect of a fines trap on the operation of a continuous stirred crystallizer. As stated in the introduction, any such analysis depends on the exact kinetics of both nucleation and growth. Such data are hard to obtain. Most published data are obtained under conditions of relatively high supersaturation and high nucleation rates; whereas in industrial crystallizers one is very often interested in large particle sizes and low nucleation rates. It is therefore difficult to compare the industrial results directly with published data. On the other hand, our results show some basic trends which are not very sensitive to the exact form of the nucleation rate, and we can compare these with general experience in industrial practice.

First, it is well known that cycling in crystallizers can be reduced or eliminated by adjusting the operation of the fines trap. The results in Figures 4 to 6 explain this by a quantitative model. The physical explanation for this stabilization is that the operation of the fines trap increases the supersaturation and therefore decreases the sensitivity parameter of the nucleation rate. This stabilization, which occurs both at constant residence time and at constant mean particle size, is due to the increase in the fraction of nuclei destroyed.

Under some conditions the value of λ (or the fraction destroyed, $1 - e^{-\lambda}$) necessary to stabilize is quite reasonable ($\lambda \approx 3$ or $1 - e^{-\lambda} \approx 0.95$). In other cases, it is quite high and the total mass of nuclei destroyed is a significant fraction (up to 30%) of the production rate. This can be seen from the general form of Figures 5 and 6, which should have the correct shape for the majority of systems, although in some special cases there could be strong deviations.

We also note that, depending on conditions, an increase of the fraction of nuclei destroyed might destabilize. In fact, we should be able, by strong increases in λ, to bring any stable crystallizer to a cycling condition. Such destabilizing effects have also been observed. In practice, destabilization due to such traps is even more common than one would expect from the results. A possible explanation might be the fact that even in mixed crystallizers some classification at the outlet occurs.

As shown in reference *16*, classification reduces the stability limit for the nucleation sensitivity. Thus, instabilities might occur at much lower values of $\lambda + b/g$ than would be predicted from an ideally mixed crystallizer.

For a point fines trap at high values of b and g the results can be given in a very simple form. If instead of b/g one uses $d\ln B_{\text{eff}}/d\ln G$, one can use the stability analysis of (*8*, *15*, *16*) without a fines trap. Thus the results

of the classified case can also be applied to the point fines trap.

For an ideally classified crystallizer (16), b/g must be less than 2. In this case stabilization by the fines trap is impractical and the fines trap would always tend to destabilize.

In a real stirred crystallizer, some classification occurs, and the initial value of $(b/g + \lambda)$ should be somewhere between 21 and 2. Its exact value can be experimentally determined. The above analysis for an ideally mixed crystallizer, while not applying quantitatively to a partially classified crystallizer, should still provide some useful guidelines to the effect of the different design parameters on the stability of the operation.

Reversing the argument, the sensitivity of the system to cycling and the dependence of cycling on the operation of the fines trap could be a very important tool in investigating B and G at low supersaturations, just as the dependence of $\bar{r}$ on θ gives us at least some partial information at lower residence times.

In addition to explaining the observed behavior of fines traps, the results presented have provided some useful guidelines for their design. In the design of such traps, r_0 and θ_0 are related by the design parameters of the baffle. The curves of Figures 4 and 5 show that for small values of r_0, $r_0/\bar{r} < 0.05$, the individual values of $\mathbf{r_0}$ and $\boldsymbol{\theta}_0$ are unimportant as long as $\mathbf{r_0}/\boldsymbol{\theta}_0$, or, equivalently, the design parameter λ, has the desired value. The designer is free to choose the best combination that he can afford.

However, in many cases low values of $\mathbf{r_0}$ are expensive to obtain, and one asks himself what value of $\mathbf{r_0}$ he can tolerate. Increasing r_0 increases the load on the heat exchanger in the fines trap, but on the other hand, a slight increase in $\mathbf{r_0}$ might have beneficial effects on stability as long as the optimum value of $\mathbf{r_0}$ is not exceeded. The final design choice is again an economic decision. The above considerations should provide some guidelines to the proper mechanical design of the fines trap.

The actual design of the trap strongly depends on the viscosity of the solution and its density, as these give the relation between r_0 and w_0. Our study indicates that in the absence of other information it is desirable to design for a range of λ between 3 and 7.

There are basically two ways in which such fines traps are designed. One can either have a large fixed recirculation through the settling zone, which keeps r_0 fixed, and adjust w_0 by changing the rate of withdrawal through the trap. Alternatively, one can withdraw directly through a settling zone; here r_0 is related to the withdrawal rate w_0, being about $w_0^{1/2}$. The relations discussed above indicate that as long as r_0 over the whole design range remains less than $0.3\,\bar{r}$, this dependence of r_0 on the withdrawal rate has no detrimental effect on the control and stabilizing action of the fines trap.

ACKNOWLEDGMENT

The work reported here was supported under NSF Grants No. GK-943 and GK-4131. Some of this work represents a portion of the research carried out by Shang-Jen Lei in partial fulfillment of the requirements for the Ph.D. degree at The City University of New York.

NOTATION

A = a dimensionless constant in Volmer's kinetics of nucleation

b = $6kB(c)G(c)^3\theta^4\,[1 + (\rho - c)B'(c)/B(c)]$, sensitivity nucleation rate

$\mathbf{B}$ = B/B_i

$B(c)$ = general nucleation rate function

C, C_i = solute concentration, and inlet solute concentration

C_s, C_m = solute saturated concentration, and a critical concentration level higher than C_s

$f(r, t)$ = number density of the crystal size distribution function

g = $6kB(c)G(c)^3\theta^4(\rho - c)G'(c)/G(c)$, sensitivity growth rate

$\mathbf{G}$ = G/G_i

$G(c)$ = general growth rate function

$h(x)$ = one form of the fines selection function, here $x = r/r_0$

$H(x)$ = a component function of the characteristic Equation (37), see Equation (38)

k = particle shape factor

K_b = rate constant of nucleation function

K_g = rate constant of growth rate function

$K(x)$ = a component function of the characteristic Equation (37), see Equation (38)

L = $(\rho - C_s)/(C_i - C_s)$

M = $(C_m - C_s)/(C_i - C_s)$

r = a characteristic linear dimension for particle

$\underline{r}$ = $r/(G\theta)$

r_0 = a critical size for fines destruction

$\mathbf{r_0}$ = $r_0/(G_i/kB_i)^{1/4}$

r^* = $r_0/(G\theta)$, a dimensionless parameter of the system

$\bar{r}$ = the weight average particle size

$\bar{\mathbf{r}}$ = $\bar{r}/(G_i/kB_i)^{1/4}$

s = $(C_i - C_s)/C_s$

t = t/θ

$\bar{t}$ = time dimension

v = the active volume of the system

w, w_0 = the volumetric throughput rate, and fines recirculated rate

x, y = dummy variables

Greek Letters

α = $6kB(c)G(0)^3\theta^4$, a parameter of linearized system

$\delta\mathbf{f}(r, t)$ = $\delta f(r, t)/(\epsilon B/G)$

$\delta\varphi$ = $\delta\varphi(t) \Big/ \left[6k\epsilon \dfrac{B}{G} (G\theta)^4(\rho - C) \right]$

ϵ = liquid volume fraction in the crystallizer

θ, θ_0 = the overall holdup time of the crystallizer, and the fines retention time

$\sigma(x)$ = $(21x^3 + 87x^2 + 128x + 64)/(x + 4)^2$

ρ = the crystal density

$\nu_n(x)$ = a dimensionless function defined in Equation (12)

φ = the total solute-crystal resource function

$\eta(r)$ = the fines selection function

λ = $r_0/(G\theta_0)$, a parameter of the fines trap

$\boldsymbol{\theta}$ = $\theta \cdot (kB_iG_i^3)^{1/4}$

$\boldsymbol{\theta}_0$ = $\theta_0(kB_iG_i^3)^{1/4}$

δ = refers to the perturbation variables of the system

Subscripts

i = refers to the variables or functions of the inlet condition

0 = pertains to the variables or parameters of the fines trap

e = refers to the steady state (equilibrium) values

LITERATURE CITED

1. Bennett, R. C., *Chem. Eng. Progr.*, **9**, 76 (1962).
2. Newman, H. H., and R. C. Bennett, *Chem. Eng. Progr.*, **3**, (1959).
3. Bennett, R. C., Swenson Evaporator Company, personal communication.
4. Bransom, S. H., and A. G. C. Palmer, *Brit. Chem. Eng.*, **10**, 672 (1964).
5. Caldwell, H. B., *Ind. Eng. Chem.*, **2**, 115 (1961).
6. Murray, D. C., and M. A. Larson, *AIChE J.*, **11**, 728 (1965).
7. Kirwan, K. J., and R. L. Pigford, *AIChE J.*, **15**, 442 (1969).
8. Randolph, A. D., and M. A. Larson, *AIChE J.*, **5**, 639 (1962); *Chem. Eng. Progr. Symp. Ser., No. 61*, 147 (1961).
9. Melia, T. P., and W. P. Moffitt, *Ind. Eng. Chem. Fundamentals*, **4**, 313 (1964).
10. Randolph, A. D., *AIChE J.*, **11**, 424 (1965).
11. Rumford, F., and J. Bain, *Trans. Inst. Chem. Engrs.*, **38**, 11 (1960).
12. Saeman, W. C., *Ind. Eng. Chem.*, **8**, 612 (1961).
13. ———, U.S. Pat. 2,883,273 (1959) and 2,737,451 (1956).
14. Schoen, H. M., *Ind. Eng. Chem.*, **8**, 607 (1961).
15. Sherwin, M. B., R. Shinnar and S. Katz, *AIChE J.*, 6, 114 (1967).
16. ———, *Chem. Eng. Progr. Symp. Ser., No. 95*, **65**, 75 (1969).
17. Ealton, Alan G., *Science*, **148**, 601 (1965).
18. Hulburt, H. M., and S. Katz, *Chem. Eng. Sci.*, **19**, 555 (1964).

APPENDIX

The Characteristic Equation Via Spectral Analysis

We sketch here the derivation of the characteristic Equations (37) and (38) for the linearized crystallizer Equations (33) and (34). Our procedure will be to write the dynamic Equations (33) and (34) in the form

$$\frac{\partial}{\partial t}\begin{Bmatrix}\delta\varphi\\ \delta f\end{Bmatrix} = \mathcal{L}\begin{Bmatrix}\delta\varphi\\ \delta f\end{Bmatrix} \tag{A1}$$

to identify the linear operator $\mathcal{L}$, and then carry out a formal spectral analysis on $\mathcal{L}$ by solving the eigenvalue problem

$$\mathcal{L}\begin{Bmatrix}\delta\varphi\\ \delta f\end{Bmatrix} = s\begin{Bmatrix}\delta\varphi\\ \delta f\end{Bmatrix} \tag{A2}$$

The conditions on s that (A2) have solutions then give just the characteristic equation (spectral equation) of the system (A1). We shall of course assess the stability of the system by whether the solutions of the spectral equation lie in the left half s-plane.

In (A1) we recognize that, apart from their dependence on t, $\delta\varphi$ is simply a scalar, but δf a function of r. Consulting Equations (33) and (34), we may accordingly write

$$\mathcal{L}\begin{Bmatrix}\delta\varphi\\ \delta f(r);\ r>0\end{Bmatrix} = \begin{Bmatrix} -\delta\varphi \\ -\dfrac{\partial[\delta f(r)]}{\partial r} - [1+R\eta(r)]\,\delta f(r) \\ \qquad + g[1+R\eta(r)]\left(e^{-r-R\int_0^r \eta}\right)\left(\delta\varphi - \int_0^\infty \frac{r^3}{6}\delta f\right);\quad r>0 \end{Bmatrix} \tag{A3}$$

being careful to complete the description of the operator by setting down the boundary condition

$$\delta f(0) + (b-g)\int_0^\infty \frac{r^3}{6}\delta f - (b-g-\alpha)\,\delta\varphi = 0 \tag{A4}$$

For Equation (A3, A4), the eigenvalue problem (A2) becomes

$$\left.\begin{aligned} &-\delta\varphi = s\cdot\delta\varphi \\ &-\frac{\partial[\delta f(r)]}{\partial r} - [1+R\eta(r)]\,\delta f(r) \\ &\quad + g[1+R\eta(r)]\,e^{-r-R\int_0^r \eta}\left(\delta\varphi - \int_0^\infty \frac{r^3}{6}\delta f\right) \\ &\qquad = s\cdot\delta f(r);\quad r>0 \\ &\delta f(0) + (b-g)\int_0^\infty \frac{r^3}{6}\cdot\delta f - (b-g-\alpha)\,\delta\varphi = 0 \end{aligned}\right\} \tag{A5}$$

From the first line of (A5) we see that either $\delta\varphi = 0$ or $s = -1$, and since we are only interested in what the eigenvalue analysis can tell us about possible instabilities, we summarily set $\delta\varphi = 0$. This leaves

$$\left.\begin{aligned} &\frac{\partial[\delta f(r)]}{\partial r} + [s+1+R\eta(r)]\,\delta f(r) \\ &\quad + g\,[1+R\eta(r)]\,e^{-r-R\int_0^r \eta}\cdot\int_0^\infty \frac{r^3}{6} \\ &\qquad \cdot\delta f = 0;\quad r>0 \\ &\delta f(0) + (b-g)\int_0^\infty \frac{r^3}{6}\cdot\delta f = 0 \end{aligned}\right\} \tag{A6}$$

Solving (A6) as a boundary value problem in $\delta f(r)$ gives

$$\delta f(r) = \lambda\cdot\exp\left\{-(s+1)\,r - R\int_0^r \eta\right\} \cdot\left(-(b-g) - g\int_0^r [1+R\eta(x)]\,e^{sx}\,dx\right);\quad r\geq 0 \tag{A7}$$

where λ is the moment integral

$$\lambda = \int_0^\infty \frac{r^3}{6}\cdot\delta f(r)\,dr$$

But λ must be computable also from the $\delta f(r)$ of Equation (A7), and this requires

$$\int_0^\infty \frac{r^3}{6}\cdot e^{-(s+1)r - R\int_0^r \eta(y)dy} \left(-(b-g) - g\int_0^r [1+R\eta(x)]e^{sx}\,dx\right)dr = 1 \tag{A8}$$

The Equation (A8) is just the characteristic equation of the system (A1), that is, of (33, 34), and can readily be rearranged into the form (37, 38).

Paper accepted September 24, 1970.